Enhancement of Ionic Conductivity and Structural Properties by 1-Butyl-3-Methylimidazolium Trifluoromethanesulfonate Ionic Liquid in Poly(vinylidene fluoride–hexafluoropropylene)-Based Polymer Electrolytes

S. Ramesh,[1] Soon-Chien Lu[2]

[1]*Centre for Ionics University Malaya, Department of Physics, Faculty of Science, University of Malaya, Kuala Lumpur 50603, Malaysia*
[2]*Centre for Surface Chemistry and Catalysis, Faculty of Bioengineering Science, Katholieke Universiteit Leuven, Leuven 3001, Belgium*

Received 28 July 2011; accepted 6 January 2012
DOI 10.1002/app.36790
Published online in Wiley Online Library (wileyonlinelibrary.com).

ABSTRACT: Polymer electrolytes (PEs) with poly(vinylidene fluoride–hexafluoropropylene) [P(VdF–HFP)] as the polymer host and doped with lithium trifluoromethanesulfonate (LiTf) and 1-butyl-3-methylimidazolium trifluoromethanesulfonate (BMIMTf) were synthesized via a solution casting method. This P(VdF–HFP)/LiTf/BMIMTf-based PE achieved about 1.8 $\times 10^{-3}$ S/cm at room temperature with 100 parts by weight (pbw) of BMIMTf. A discrepancy was observed when 25 pbw of BMIMTf was doped into the system and was related to the reactivity of Li^+ and 1-butyl-3-methylimidazolium cation ($BMIM^+$), which could be corroborated with differential scanning calorimetry scans. Fourier transform infrared spectroscopy and X-ray diffraction revealed the role of P(VdF–HFP) as merely a mechanical support with no direct interaction with BMIMTf. Photoluminescence was also used to detect structural alterations in the local environment of PE. © 2012 Wiley Periodicals, Inc. J. Appl. Polym. Sci. 000: 000–000, 2012

Key words: differential scanning calorimetry (DSC); FTIR; noncrystalline polymers; thermal properties; thin films

INTRODUCTION

A polymer electrolyte (PE) is a solvent-free system where the ionically conducting phase is formed by the dissolution of salts in a high-molecular-weight polymer matrix. It is now employed in the design of a few types of lithium polymer batteries. These are rechargeable batteries, which have technologically evolved from lithium-ion batteries. At the same time, PEs can be used as separators in lithium batteries because of their thermal and chemical stabilities. They provide enhanced safety at the price of moderate room-temperature ionic conductivity, and this obstructs their use for wider battery applications.[1] However, driven by their potential applications in a variety of electronic devices, there have been numerous studies on the development and understanding of the mechanism of ion conduction in PE.[2]

Ionic conductivity is generally regarded as a property of the amorphous phase, and in addition, ionic association, ion–polymer interactions, and local relaxations of the polymer strongly influence the ion mobility.[3] A basic understanding of the polymer host and additive structures that offer high ionic conductivity is needed to obtain chemical and mechanical stability.[4] The ion mobility in a polymer matrix is essentially different from that in the case of an organic liquid or aqueous electrolyte[5] and, therefore, requires a different approach of investigation.

In this study, we incorporated 1-butyl-3-methylimidazolium trifluoromethanesulfonate (BMIMTf) ionic liquid into a poly(vinylidene fluoride–hexafluoropropylene) [P(VdF–HFP)]/lithium trifluoromethanesulfonate (LiTf)-based PE system. The ionic liquid–PE has been reported to have a number of beneficial properties, including (1) a high ionic conductivity, (2) wide electrochemical windows, (3) negligible volatility, (4) nonflammability, and (v) subambient temperature operation.[6] P(VdF–HFP) was chosen because it consists of two kinds of monomers: one is symmetrical VdF, and the other is asymmetrical

Correspondence to: S. Ramesh (rameshtsubra@gmail.com).
Contract grant sponsor: Fundamental Research Grant Scheme from Ministry of Higher Education, Malaysia; contract grant number: FP009/2010B.
Contract grant sponsor: Universiti Malaya; contract grant number: UMRG: RG140-11AFR.

hexafluoropropylene. Combining these two kinds of monomers gives mechanical strength and ionic conductivity at the same time because of their molecular structures. We wished to further study this kind of ionic-liquid-based PE in other aspects, such as its structural and thermal properties, with the help of horizontal attenuated total reflectance (HATR)–Fourier transform infrared (FTIR) spectroscopy, X-ray diffraction (XRD), differential scanning calorimetry (DSC), and photoluminescence (PL) spectroscopy.

EXPERIMENTAL

Materials

P(VdF–HFP), with a weight-average molecular weight of 455,000, was obtained from Sigma-Aldrich (St. Louis, Missouri, USA). LiTf (Fluka, Philipp Friedrich Hiller, Steinheim, Germany) salt was obtained from Acros and was dried at 100°C for 1 h to eliminate trace amounts of water in the material before the preparation of PEs. BMIMTf (Sigma-Aldrich, St. Louis, Missouri, USA) was obtained from Agro Organics. Acetone (analytical-reagent grade) was obtained from J. T. Baker.

Preparation of PEs

PE complexes were prepared with compositions according to its ratio of ionic liquid in parts by weight (pbw), ranging from 25 to 100 pbw, with a fixed ratio of polymer and lithium salt of 60/40 pbw. In this study, a solution casting technique was employed to obtain polymer samples with acetone as a solvent. The thoroughly stirred mixture was then cast onto a Petri dish and allowed to evaporate slowly inside a fume hood. This procedure yielded mechanically stable and free-standing PEs. The resulting polymer films were labeled LB-0 to LB-100, with the number after the hyphen designating the amount of BMIMTf in pbw doped into each sample. The thickness of the polymer films was measured with a micrometer screw gauge (Mitutoyo, Japan).

Instrumentation

The samples were cut out to resemble the shape of the stainless steel blocking electrodes used in this study and were sandwiched between them. A HIOKI 3532-50 LCR Hi-Tester (Ueda, Nagano, Japan) was used to perform the impedance measurements for each PE over the frequency range of 50 Hz to 1 MHz. The equation $\sigma = l/R_bA$ was used to calculate the ionic conductivity of the polymer film sample, where σ is the conductivity (S/cm), l is the thickness of the polymer film sample (cm), R_b is the bulk resistance (Ω) obtained from the Cole–Cole impedance plot, and A is the surface area of the stainless steel blocking electrodes (cm^2).

The HATR–FTIR spectroscopy studies were carried out with PerkinElmer FTIR Spectrum RX1 spectrometer with an HATR accessory in the wave-number regions of 4000–2600 and 1800–650 cm^{-1}, with a resolution of 4 cm^{-1}. Also, there were no signs of a carbonyl band from residual acetone around 1700 cm^{-1}.

The XRD (Bruker AXS, Karlsruhe, Germany) patterns were analyzed with a Siemens D-5000 diffraction system with Cu Kα radiation at a wavelength of 1.5406 Å. The diffraction pattern was recorded at room temperature for Bragg angles (2θ's) varying from 10 to 80°.

DSC (Polaris Parkway, Columbus, OH, USA) was also performed with a Mettler–Toledo analyzer that consisted of a DSC823^e main unit and STARe software. Approximately 2 mg of sample was sealed in a standard 40-μL aluminum pan. The sample was then heated sequentially from 30 to 100°C, remained for 1 min, and was then cooled down to 30°C to eliminate the trace amount of water absorbed into the sample. It was then reheated up to 200°C and again cooled down to 30°C. A heating rate of 10°C/min was applied for the heating and cooling cycles. All of the measurements were conducted in a nitrogen atmosphere.

A PerkinElmer (FTIR: Waltham, Massachusetts, United States) LS55 luminescence spectrometer was used for the PL measurements. The sample holder was placed at 60° against the excitation wavelength. The excitation and emission wavelengths were set at 280 and 360 nm, respectively.

RESULTS AND DISCUSSION

AC impedance spectroscopy

Figure 1 shows Cole–Cole impedance plot of samples LB-0, LB-25, LB-50, and LB-100 at room temperature. As already mentioned in the Experimental section, the conductivity of the PEs could be calculated from the equation $\sigma = l/R_bA$. To determine the bulk resistance, Cole–Cole impedance plots were obtained, with the x axis as the real impedance and the y axis as the imaginary impedance. We determined the bulk resistance by reading the point on the real axis closest to zero in the plots. This analysis method is typical for the measurement of the conductivity in membranes.[7] As shown in Figure 1(a,b), the shape of the impedance plot changed instantaneously when 25 pbw of BMIMTf was added to the system; this suggested changes in the conducting pathways. It then slowly changed back to the same shape but different magnitude when more ionic liquid was added, as shown in Figure 1(d).

Figure 2 illustrates the variation of the ionic conductivity as a function of the BMIMTf content doped into the P(VdF–HFP)–LiTf-based PE system. LB-25,

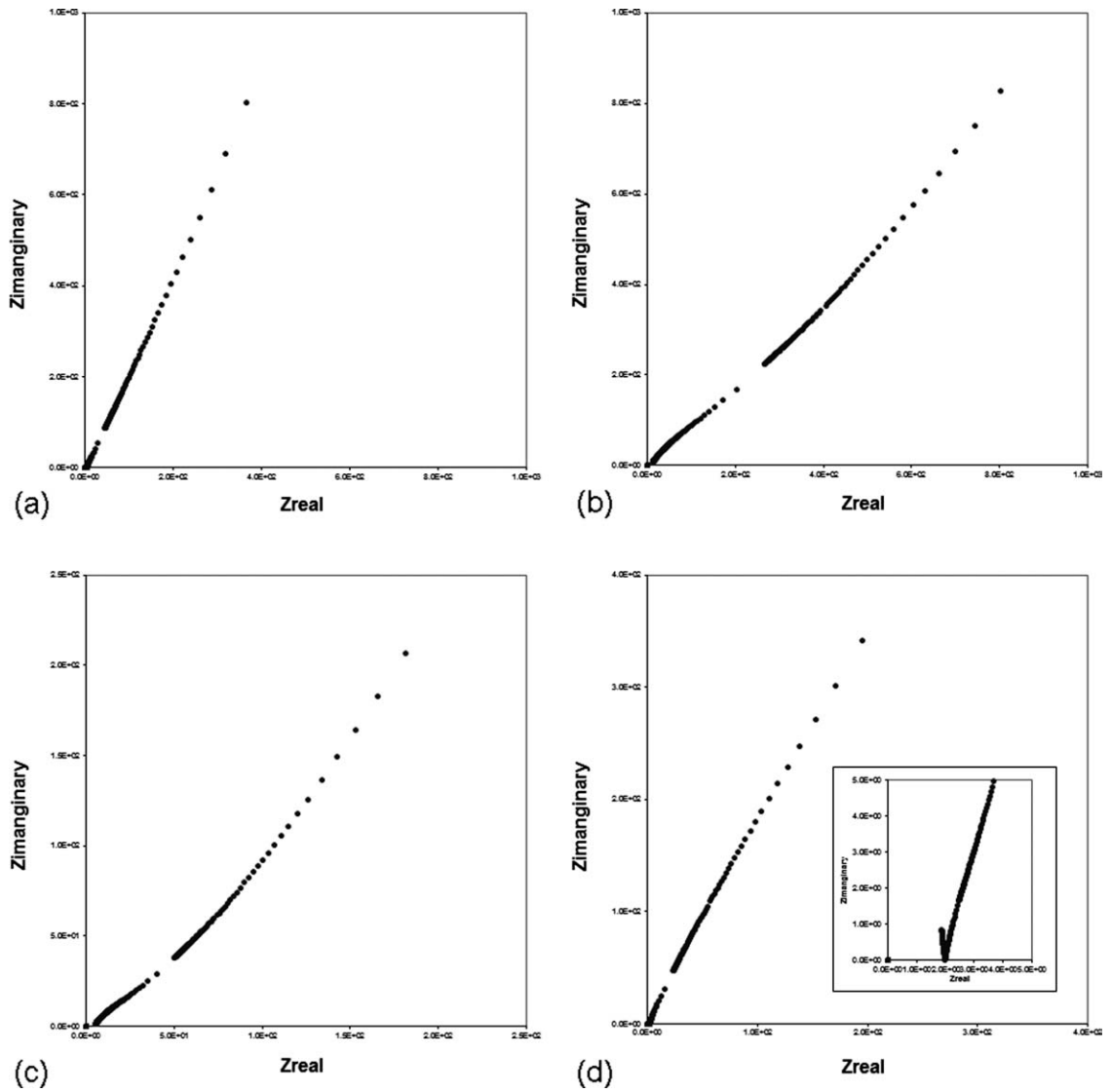

Figure 1 Cole–Cole impedance plot of samples (a) LB-0, (b) LB-25, (c) LB-50, and (d) LB-100 at room temperature. The magnified axis of LB-100 in a higher frequency region is shown in the inset. Z_{real} is the real part of complex impedance; $Z_{imaginary}$ is imaginary part of complex impedance.

the PE sample with 25 pbw of BMIMTf incorporated into it, showed the lowest ionic conductivity among all if the samples, about 2.0 $\times 10^{-4}$ S/cm at room temperature. On the other hand, LB-100, the PE sample with 100 pbw of BMIMTf incorporation, achieved the highest ionic conductivity in this series, about 1.8 $\times 10^{-3}$ S/cm under the same conditions. The relatively high ionic conductivity of PE might have been due to the intrinsically high ionic conductivity of neat BMIMTf, as it was already in ionic form.[8] Even though both samples had sufficient ionic conductivity for lithium battery applications, it was important to study the trend of ionic conductivity to find the optimum conditions for this system.

As shown in Figure 2, the ionic conductivity of PE decreased when the first 25 pbw of BMIMTf was added to the system; then, it went back to slightly higher than the LB-0 sample without ionic liquid and increased with the further addition of BMIMTf. This was not so unusual, as the ionic conductivity was expected to be enhanced instantaneously with the inclusion of ionic liquid. Both anions and cations

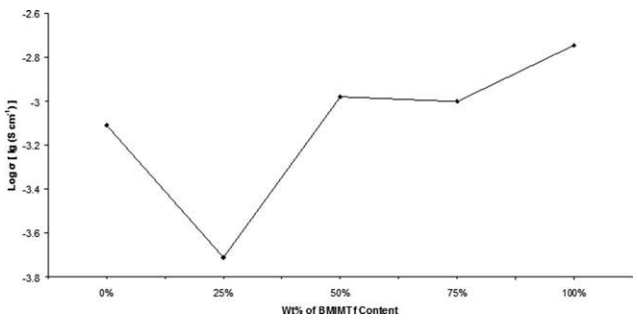

Figure 2 Variation of the ionic conductivity as a function of the BMIMTf content at room temperature.

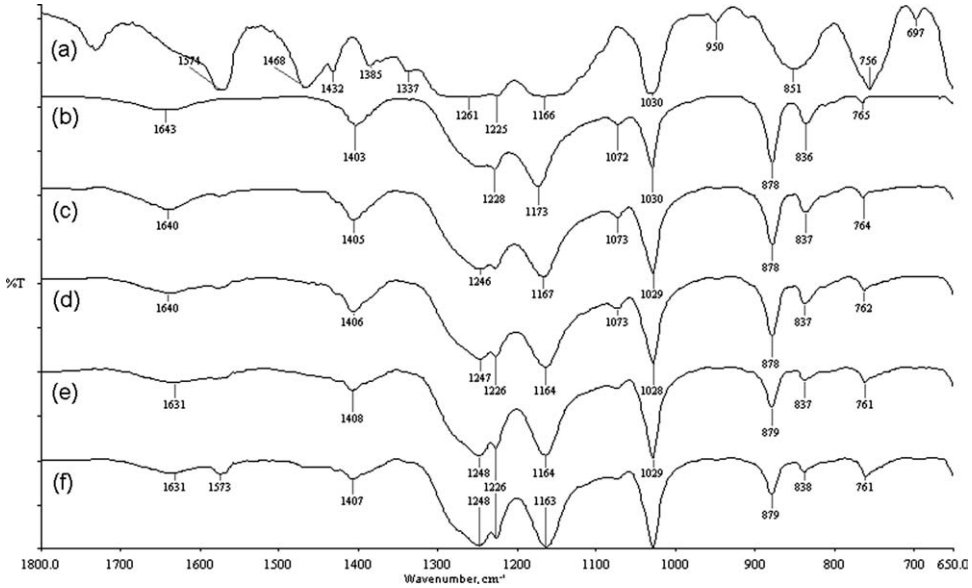

Figure 3 HATR–FTIR spectra of (a) BMIMTf, (b) LB-0, (c) LB-25, (d) LB-50, (e) LB-75, and (f) LB-100 in the wave-number region 1800–650 cm^{-1}.

in LiTf and BMIMTf could be conducting species with their dissociative ionic forms in this system. However, the discrepancy found in LB-25 could be explained as a competition between Li^+ and $BMIM^+$ to reassociate with trifluoromethanesulfonate anion (Tf^-), as there was only one sort of anion. Apparently, Li^+ was far smaller in size, and in view of the bonding orientation, it achieved a more stable form of neutral ion pair with Tf^- compared to $BMIM^+$. When BMIMTf was first introduced into the system, Li^+ won the battle as it outnumbered the amount of $BMIM^+$ and, thus, lowered the ionic conductivity. This supposition was corroborated by DSC, which showed that LB-25 possessed a higher melting temperature (T_m) than LB-0, as discussed in a later section. This observation also suggested the molecular-level blending of BMIMTf with P(VdF–HFP), as the ionic conductivity would not be decreased to such an extent if the blending was at microscopic rather than molecular level.[9]

However, when the quantity of $BMIM^+$ was increased, in this case, when 50, 75, and 100 pbw of BMIMTf were added to the system, it started to act like a plasticizer, to transform the crystalline phase of P(VdF–HFP) to the amorphous phase; this helped in the ionic dissociation of LiTf and significantly reduced PE's resistance, where the effect was more pronounced at low temperatures.[10] Also, both $BMIM^+$ and Tf^- were mobile and contributed to the overall ionic conductivity of PE.[11] Other than that, the BMIMTf used in this study had a low viscosity. It has been reported that the ionic conductivity is more dependent on the mobility of free ions and tortuosity of the ion conduction pathway than the number of free mobile ions once PE reaches a high ionic conductivity.[12] It has already been shown that the crystallinity of the medium, which in turn, is related to the ion mobility, is the main controlling factor of ionic conductivity.[13] All these factors made the ionic conductivity increase again with greater amounts of ionic liquid.

HATR–FTIR spectroscopy

FTIR spectroscopy is vital in the examination of interactions taking place between individual constituents in a PE system. PE's bands in these HATR–FTIR spectra varied as a result of the mixture of different composition ratios and the occurrence of complexation between them. With the HATR accessory, the FTIR spectra could be obtained directly from the resulting PE samples of this work without their redissolution with acetone; this eliminated the influence of the solvent. The absence of residual acetone was proven, as there were no signs of a carbonyl band around 1700 cm^{-1}.

The HATR–FTIR spectra of BMIMTf, LB-0, LB-25, LB-50, LB-75, and LB-100 from the wave-number regions 1800–650 and 4000–2600 cm^{-1} are shown in Figures 3 and 4, respectively. All spectra were recorded in transmittance mode. Some of the possible band assignments for pure P(VdF–HFP), LiTf, and BMIMTf have already been reported in literature[14–19] and are listed in Table I. The bands corresponding to Tf^- in BMIMTf are not included in the table to avoid redundancy, as they were similar to those for LiTf.

From both Figures 3 and 4, it seems that the spectrum of LB-25 was fairly undisturbed, even with the incorporation of BMIMTf, except for the band at

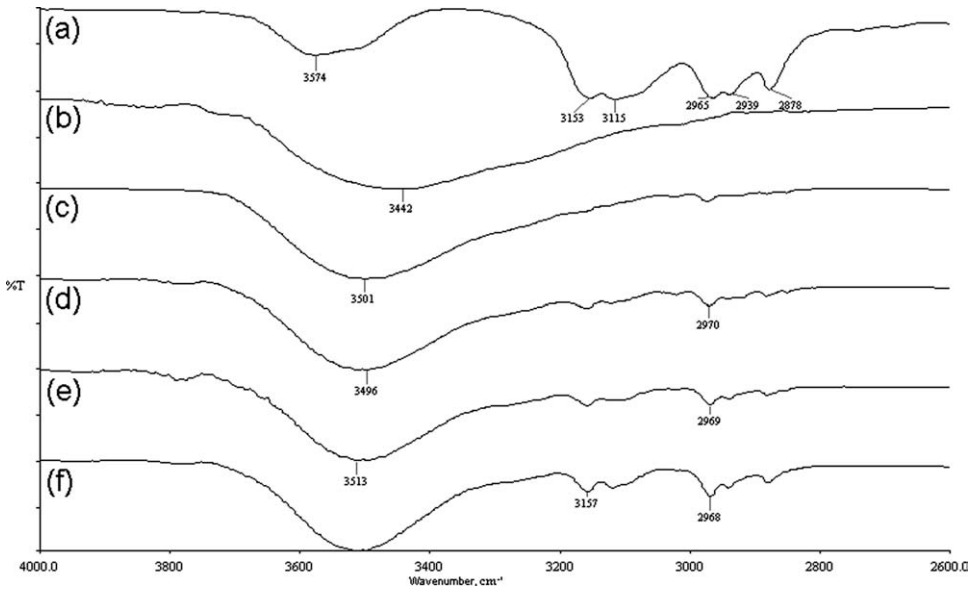

Figure 4 HATR–FTIR spectra of (a) BMIMTf, (b) LB-0, (c) LB-25, (d) LB-50, (e) LB-75, and (f) LB-100 in the wave-number region 4000–2600 cm^{-1}.

3442 cm^{-1}, which was caused by moisture being absorbed in the materials, maybe because of overlapping with the CH stretching band of BMIMTf at 3574 cm^{-1}. On the other hand, many bands of BMIMTf were suppressed vividly and only reappeared at higher concentrations when it was added to the P(VdF–HFP)–LiTf system, including bands at 756, 851, 1468, 1574, 2878, 2939, 2964, 3115, and 3574 cm^{-1}. This may indicate that drastic changes took place in BMIMTf, most probably bonding sites and bonding strength. Given the facts that most of the bands corresponding to BMIMTf remained relatively unchanged when they reemerged at higher concentrations and that characteristic peaks of P(VdF–HFP) did not shift much with the inclusion of BMIMTf, we deduced that BMIMTf did not have much direct interaction with the polymer but seemingly had some interaction with LiTf, which was not observable in these IR spectra, as there must have been some kind of interaction to have caused such a trend in the ionic conductivity. Because it has been suggested that the polymer in PE does not play an active role in the ionic conduction process and acts as a stiffener only,[20] BMIMTf only affected the intensity of the peaks corresponding to the amorphous region in P(VdF–HFP) to a small extent. This was commensurate with the justification given earlier, where $BMIM^+$ competed with Li^+ to form a neutral ion pair with Tf^- and changed the crystallinity at higher concentrations, where P(VdF–HFP) was not involved.

XRD analysis

Besides infrared spectroscopy, which was already described in the previous section, XRD analysis was also employed to verify the interaction or complexation among P(VdF–HFP), LiTf, and BMIMTf.[21] Changes, such as a shifting of peaks, decreasing of

TABLE I
Possible Assignments of Some Significant Peaks in the HATR–FTIR Spectra of P(VdF–HFP), LiTf, and BMIMTf

Compound	Wave number (cm^{-1})	Possible assignment
LiTf	765	Symmetrical deformation mode of CF_3
	1032	Symmetrical stretching of SO_3
	1179, 1259	Asymmetrical stretching of SO_3
	1229	Symmetrical vibration of CF_3
	1638	Characteristic peak of Tf^-
P(VdF–HFP)	760, 853	α phase
	794	CF_3 stretching
	836, 871	Amorphous region
	1062	C—C skeletal vibration
	1179	Symmetrical stretching of —CF_3
	1202	Asymmetrical stretching of —CF_2—
	1400	—C—F— stretching
BMIMTf	697	Symmetrical bending of NH
	851	In-plane bending of the imidazole ring
	950	In-plane bending of CNC
	1337	Symmetrical bending in-plane of CH
	1432	HCC deformation
	1468	Symmetrical in-plane bending of the imidazole ring
	1574	HCN deformation
	2878, 2939	Aliphatic *n*(C—H)
	2965	CH stretching in the methyl group
	3115, 3152	=C—H stretching
	3574	CH stretching

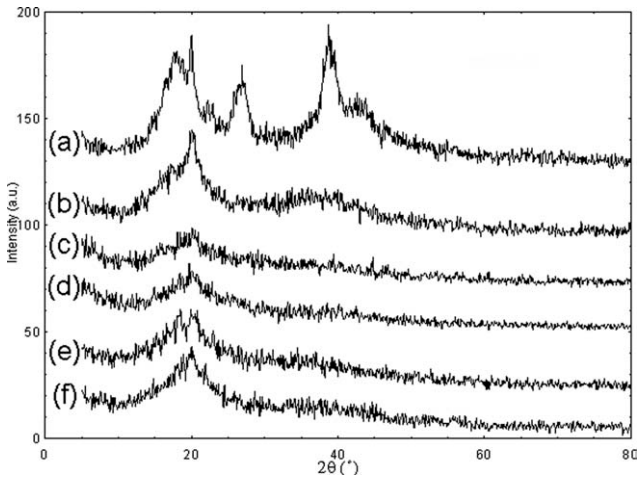

Figure 5 X-ray diffractograms of (a) P(VdF–HFP), (b) LB-0, (c) LB-25, (d) LB-50, (e) LB-75, and (f) LB-100.

peaks, or broadening of peaks, can be evidence of the occurrence of complexation between the constituents in a system.[22] Figure 5 shows the X-ray diffractograms of P(VdF–HFP), LB-0, LB-25, LB-50, LB-75, and LB-100.

In Figure 5(a), the four peaks that were found at $2\theta = 18.0$, 20.0, 26.9, and 38.8° in P(VdF–HFP) correspond to the (100), (020), (110), and (021) characteristic crystalline peaks of PVdF.[23] This suggested the coexistence of a multiphase system having partial crystallization of PVdF units along with an amorphous polyhexafluoropropylene phase and gave a semicrystalline structure of P(VdF–HFP).[24] Although there was no discernible change in the peaks in the XRD patterns observed when LiTf was incorporated into the system, three intense peaks at $2\theta = 18.0$, 26.9, and 38.8° disappeared instantaneously; this implied complexation, good compatibility between the two constituents, and a decrease in the crystallinity of the samples. The increase in the amorphous phase in the sample was apparent from the appearance of a broadening of the diffraction peaks, especially at $2\theta = 38.8°$.

The observation was almost the same as that discussed previously when 25 pbw of BMIMTf was first added to LB-25, just with a further broadening of the peaks compared with LB-0. This suggested that BMIMTf most likely blended with P(VdF–HFP)–LiTf at molecular level, like what was described earlier, acting like plasticizer and stamping out the remaining semicrystalline structure of this copolymer without complexation. The rather uniformly amorphous microstructure of the resultant PE should be advantageous for its ionic conductivity and flexibility.[9] Nevertheless, its partial crystalline nature still persisted, as was evident from the observation of the predominant peak at $2\theta = 20.0°$, and it functioned as a mechanical support for the PE.

On the other hand, there was a divergence when BMIMTf was added to the system to a greater extent. The peak at $2\theta = 20.0$, which was already suppressed when 25 pbw of BMIMTf was incorporated, got increasingly intense when 50, 75, and 100 pbw of the same ionic liquid were added. In accordance with the results reported in earlier sections, we believed the peak arose from the free ions of BMIMTf. This indicated that there were free ions, which did not complex or have interaction with P(VdF–HFP) or LiTf because of the excessive amount of ionic liquid.[25] Thus, it functioned as a plasticizer to decrease the crystallinity of the polymer matrix, promoted the migration of ions, and eventually improved the ionic conductivity. Other than that, other polymer additives, such as liquid electrolytes and silicon nanowires, to improve PEs with better electrochemical and mechanical performance are also found in the literature.[26,27]

DSC

Other than FTIR and XRD, DSC is yet another important technique for authenticating the occurrence of interactions or complexation between constituents in a PE system.[28] Concurrently, other parameters, such as the crystallinity, thermal stability, T_m, and crystallization temperatures, can be obtained from the same procedure. These parameters are essential, for example, to determine the overall separator properties of the PE material when it is operated in a battery system.[29] Figures 6 and 7 illustrate the DSC thermograms of LB-0, LB-25, LB-50, LB-75, and LB-100 in heating and cooling runs, respectively.

T_m of pristine P(VdF–HFP) (not shown) was found to be 137°C, which was very close to that reported in the literature.[30] The heating run DSC thermograms shown in Figure 6 reveal a decrease in T_m, from approximately 144 to 135°C, when BMIMTf was included in the PE system. However, it was accompanied with a somewhat irregular trend of T_m, in conjunction with a broadening of melting peaks. It rose to a slightly higher temperature when 25 pbw of BMIMTf was added and then continued to drop up to 100 pbw of BMIMTf. The increase could be interpreted as explained earlier, where ionic reassociation or the more commonly known ion-pair effect between Li^+ and Tf^- took place in LB-25, and thereby, a higher energy was needed. It could also be explained as a small change happening in the polymer crystal phases, such as changes from the dominant α phase to the coexistence of α-, β-, and γ-phase crystals.[31] On the other hand, the decrease in T_m and the broadening of the melting endotherms could be ascribed to the presence of BMIMTf, which led to an inhibition of effective reorganization of PVdF for crystallization to occur and, thus, lowers

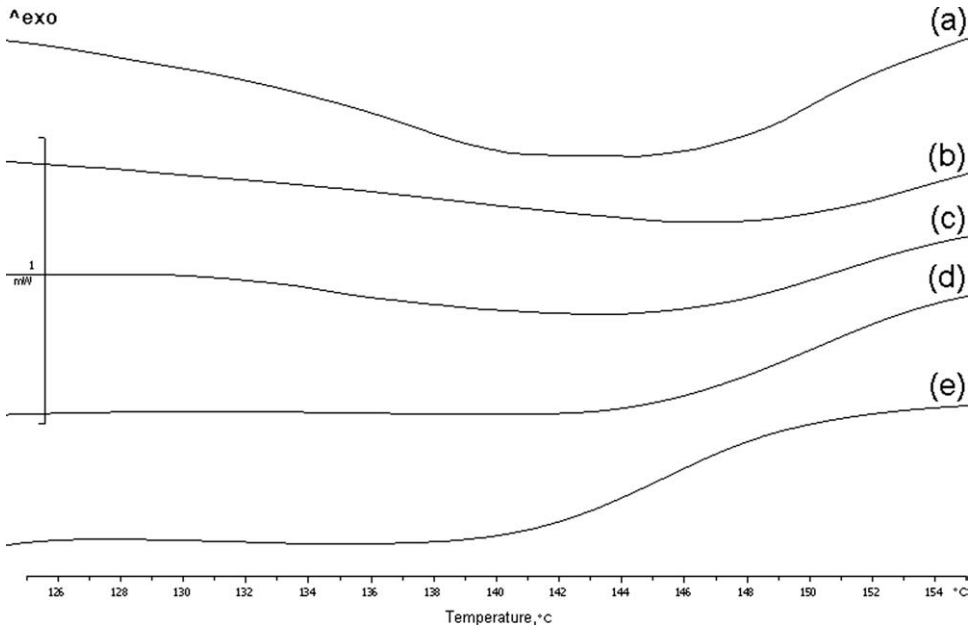

Figure 6 Differential scanning calorimetric thermograms of (a) LB-0, (b) LB-25, (c) LB-50, (d) LB-75, and (e) LB-100 in the heating run.

the crystallinity. For a PE system with the incorporation of an ionic liquid, the temperature range where it remains in the same phase, that is, before melting occurs, is rather wide, from at least 30 to 130°C. This is highly favorable, as a wide operating temperature range is vital for many battery applications, such as military and aerospace applications and electric and hybrid vehicle applications.[9]

As for the cooling run, it was clear that when the BMIMTf content was increased, the crystallization exotherms decreased in height and shifted toward lower temperatures, as shown in Figure 7. This may have been due to the crystallinity decreases as BMIMTf content increased,[32] and this result could be validated with the calculation of crystallinity (X_C) from the cooling DSC thermograms with the following equation:

$$X_C = \left(\frac{\Delta H_m}{\Delta H_m^{\theta}}\right) \times 100\%$$

where ΔH_m is the heat of fusion of the sample and $\Delta H_m\theta$ is the reference heat of fusion of the

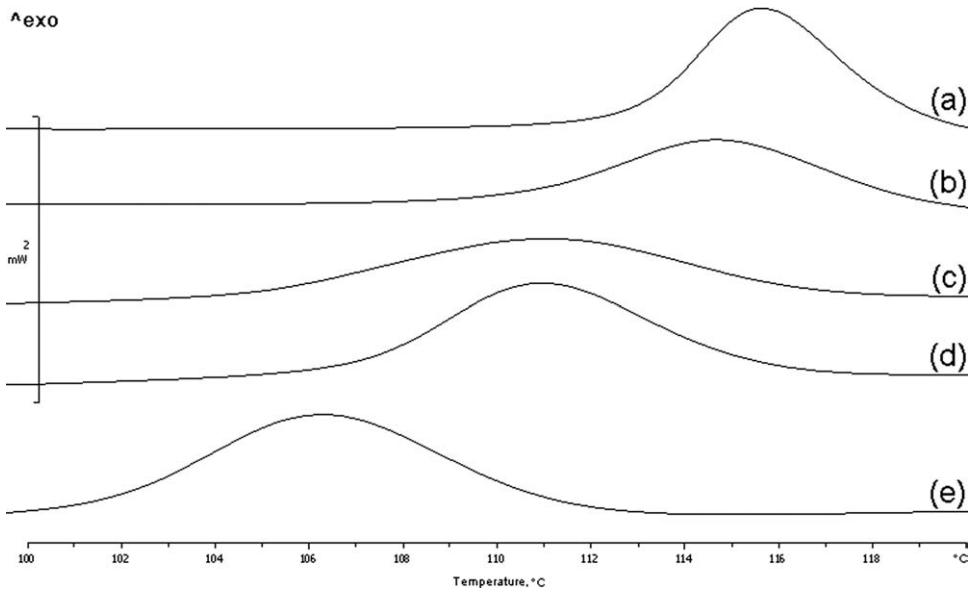

Figure 7 Differential scanning calorimetric thermograms of (a) LB-0, (b) LB-25, (c) LB-50, (d) LB-75, and (e) LB-100 in the cooling run.

crystalline α-PVdF (105 J/g).[33] The result is tabulated in Table II and shows good agreement with the previous suggestion. The lower crystallization temperature values implied that the temperature range over which they could exist stably in an amorphous state became wider.[34]

PL spectroscopy

As discussed previously, the ionic conductivity can be related to the ion mobility, which is strongly associated with the crystallinity. In PEs with low crystallinity, conducting species within the sample should have a higher mobility to give greater ionic conductivity. It is generally accepted that in conventional PE, the conducting cations are coordinated by strongly electron-withdrawing constituents. In this study, this would have been fluorine in the P(VdF–HFP) backbone. Thus, ionic conduction was strongly coupled with the segmental motions of the polymer matrix, which were closely correlated with local free volume and local viscosity around the charge-transporting ions.[35] It has been shown that fluorescence studies can provide information on the local viscosity in PEs, which is termed the *microviscosity*.[36] Also, this technique can also be used to detect structural alterations in the local environment,[37] which was the objective of this study.

PL emission and excitation spectra of pure P(VdF–HFP), LB-0, LB-25, LB-50, LB-75, and LB-100 are shown in Figure 8(a,b), respectively. No obvious changes were noted for both fluorescence spectra of LB-0, except in the intensity, which was understandable, as dopants tend to reduce the prominent peaks of an undoped sample.[38] However, the spectra changed significantly when BMIMTf was added to the system; this included new peaks at approximately 430 and 280 nm in the emission and excitation spectra, respectively. Presumably, it was a material with certain luminescent characteristics, as it has been employed extensively in the research of electrochromic devices. In addition, it seemed that the intensity increased with increasing amount of BMIMTf. This suggested phase changes in the polymer matrix and that a higher degree of free ionic motion, or simply ion mobility, was observed when a greater amount of BMIMTf was incorporated into the P(VdF–HFP)–LiTf system. The enhancement of ion mobility was attributed to the addition of BMIMTf, which disrupted the crystalline phase of P(VdF–HFP) and restructured it to the amorphous phase.

TABLE II
Calculated Crystallinity Values of LB-0, LB-25, LB-50, LB-75, and LB-100

Sample	Crystallinity (%)
LB-0	10.16
LB-25	6.02
LB-50	5.45
LB-75	4.35
LB-100	3.89

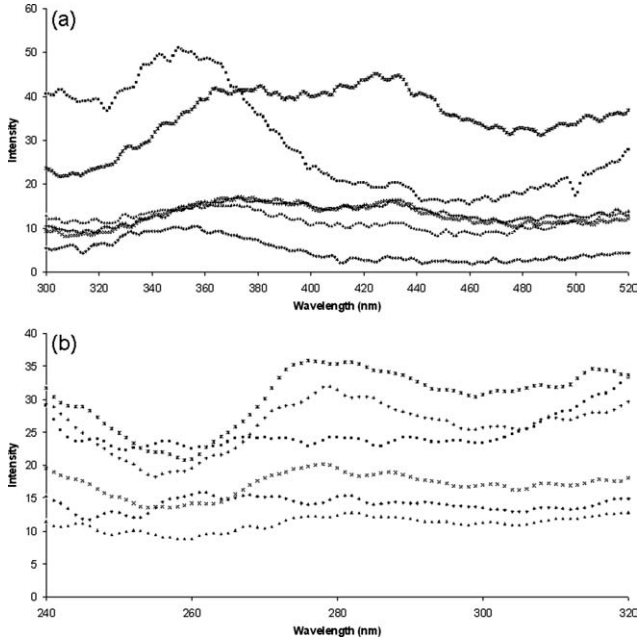

Figure 8 PL (a) emission and (b) excitation spectra of (◆) P(VdF–HFP), (■) LB-0, (▲) LB-25, (×) LB-50, (+) LB-75, and (*) LB-100.

CONCLUSIONS

The presence of BMIMTf in the system was shown to be favorable toward the electrochemical, structural, and thermal properties of the P(VdF–HFP)–LiTf-based PE system. When 100 pbw of BMIMTf was incorporated into the system, it achieved a conductivity of about 1.8 $\times 10^{-3}$ S/cm at room temperature; this is ample for many portable electronic devices. Even though a discrepancy was observed when 25 pbw of BMIMTf was added, it could be explained by the competition between Li^+ and $BMIM^+$ to reassociate with Tf^- and was corroborated with DSC scans. FTIR spectroscopy and XRD revealed the role of P(VdF–HFP) as merely a mechanical support with no direct interaction with BMIMTf. However, it was the combination of amorphosity and crystallinity that makes P(VdF–HFP) a high potential candidate with great prospects in PE research. PL was also employed to detect structural alterations in the local environment of the PE.

References

1. Ahmad, S.; Agnihotry, S. A. Curr Appl Phys 2009, 9, 108.
2. Karan, N. K.; Pradhan, D. K.; Thomas, R.; Natesan, B.; Katiyar, R. S. Solid State Ionics 2008, 179, 689.

3. Silva, R. A.; Silva, G. G.; Moreira, R. L.; Pimenta, M. A. Phys Chem Chem Phys 2003, 5, 2424.
4. Suthanthiraraj, S. A.; Kumar, R.; Paul, B. J. Spectrochim Acta Part A 2009, 71, 2012.
5. Huang, W. W.; Frech, R.; Wheeler, R. A. J Phys Chem 1994, 98, 100.
6. Fuller, J.; Breda, A. C.; Carlin, R. T. J Electroanal Chem 1998, 459, 29.
7. Marschall, R.; Rathousky, J.; Wark, M. Chem Mater 2007, 19, 6401.
8. Lee, J. S.; Nohira, T.; Hagiwara, R. J Power Sources 2007, 171, 535.
9. Xu, J. J.; Ye, H.; Huang, J. Electrochem Commun 2005, 7, 1309.
10. Choi, J.-W.; Cheruvally, G.; Kim, Y.-H.; Kim, J.-K.; Manuel, J.; Raghavan, P.; Ahn, J.-H.; Kim, K.-W.; Ahn, H.-J.; Choi, D. S.; Song, C. E. Solid State Ionics 2007, 178, 1235.
11. Singh, P. K.; Kim, K.-W.; Rhee, H.-W. Electrochem Commun 2008, 10, 1769.
12. Choi, N.-S.; Lee, Y. M.; Lee, B. H.; Lee, J. A.; Park, J.-K. Solid State Ionics 2004, 167, 293.
13. Bhattacharya, B.; Lee, J. Y.; Geng, J. X.; Jung, H.-T.; Park, J.-K. Langmuir 2009, 25, 3276.
14. Ramesh, S.; Chai, M. F. Mater Sci Eng B 2007, 139, 240.
15. Li, Z. H.; Zhang, H. P.; Zhang, P.; Li, G. C.; Wu, Y. P.; Zhou, X. D. J Membr Sci 2008, 322, 416.
16. Sadlej, J.; Jaworski, A.; Miaskiewicz, K. J Mol Struct 1992, 274, 247.
17. Chowdhury, A.; Thynell, S. T. Thermochim Acta 2006, 443, 159.
18. Rao, G. R.; Rajkumar, T.; Varghese, B. Solid State Sci 2009, 11, 36.
19. Tatara, W.; Wójcik, M. J.; Lindgren, J.; Probst, M. J Phys Chem A 2003, 107, 7827.
20. Kumar, R.; Sekhon, S. S. Ionics 2004, 10, 10.
21. Ramalingaiah, S.; Reddy, D. S.; Reddy, M. J.; Laxminarsaiah, E.; Rao, U. V. S. Mater Lett 1996, 29, 285.
22. Ramesh, S.; Lim, J. Y. Ionics 2009, 15, 725.
23. Stephen, A. M.; Nahm, K. S.; Kulandainathan, M. A.; Ravi, G.; Wilson, J. Eur Polym J 2006, 42, 1728.
24. Saika, D.; Kumar, A. Electrochim Acta 2004, 49, 2581.
25. Jeong, S.-K.; Jo, Y.-K.; Jo, N.-J. Electrochim Acta 2006, 52, 1549.
26. Zhang, H. P.; Zhang, P.; Li, Z. H.; Sun, M.; Wu, Y. P.; Wu, H. Q. Electrochem Commun 2007, 9, 1700.
27. Zhang, P.; Yang, L. C.; Li, L. L.; Ding, M. L.; Wu, Y. P.; Holze, R. J Membr Sci 2011, 379, 80.
28. Sirisopanaporn, C.; Fernicola, A.; Scrosati, B. J Power Sources 2009, 186, 490.
29. Abbrent, S.; Plestil, J.; Hlavata, D.; Lindgren, J.; Tegenfeldt, J.; Wendsjö, A. Polymer 2001, 42, 1407.
30. Ulaganathan, M.; Pethaiah, S. S.; Rajendran, S. Mater Chem Phys 2011, 129, 471.
31. Sajkiewicz, P. Eur Polym J 1999, 35, 1581.
32. Vickraman, P.; Aravindan, V.; Shankarasubramaniam, N. Ionics 2007, 13, 355.
33. Choi, S. W.; Jo, S. M.; Lee, W. S.; Kim, Y.-R. Adv Mater 2003, 15, 2027.
34. Ji, K.-S.; Moon, H.-S.; Kim, J.-W.; Park, J.-W. J Power Sources 2003, 117, 124.
35. Park, U.-S.; Hong, Y.-J.; Oh, S. M. Electrochim Acta 1996, 41, 849.
36. Jeon, S. M.; Bae, S. C.; Turner, J.; Granick, S. Polymer 2002, 43, 4651.
37. Waldow, D. A.; Ediger, M. D.; Yamaguchi, Y.; Matsushita, Y.; Noda, I. Macromolecules 1991, 24, 3147.
38. Anandan, S.; Radhakrihna, S. Polymeric Materials; Radhakrihna, S., Arof, A. K., Eds.; Narosa: New Delhi, India, 1998; p 181.